Journal of Medicinal Chemistry

Article

pubs.acs.org/jmc

Design, Synthesis, and Biological and Crystallographic Evaluation of Novel Inhibitors of *Plasmodium falciparum* Enoyl-ACP-reductase (*Pf*FabI)

Federica Belluti,*[,†,∞] Remo Perozzo,*[,‡,∞] Leonardo Lauciello,[‡] Francesco Colizzi,[§] Dirk Kostrewa,[∥] Alessandra Bisi,[†] Silvia Gobbi,[†] Angela Rampa,[†] Maria Laura Bolognesi,[†] Maurizio Recanatini,[†] Reto Brun,[⊥] Leonardo Scapozza,[‡] and Andrea Cavalli[†,#]

[†]Department of Pharmacy and Biotechnology, University of Bologna, Via Belmeloro 6, I-40126 Bologna, Italy

[‡]Pharmaceutical Biochemistry Group, School of Pharmaceutical Sciences, University of Geneva, University of Lausanne, Quai Ernest-Ansermet 30, CH-1211 Geneva 4, Switzerland

[§]International School for Advanced Studies, Via Bonomea, 265, I-34136 Trieste, Italy

[∥]Department of Biochemistry, Gene Center Munich, Ludwig-Maximilians-University Munich, Munich 81377, Germany

[⊥]Swiss Tropical & Health Institute, Socinstrasse 57, CH-4002 Basel, Switzerland

[#]Department of Drug Discovery and Development, Istituto Italiano di Tecnologia, Via Morego 30, I-16163 Genova, Italy

Supporting Information

ABSTRACT: Malaria, a disease of worldwide significance, is responsible for over one million deaths annually. The liver-stage of *Plasmodium's* life cycle is the first, obligatory, but clinically silent step in malaria infection. The *P. falciparum* type II fatty acid biosynthesis pathway (*Pf*FAS-II) has been found to be essential for complete liver-stage development and has been regarded as a potential antimalarial target for the development of drugs for malaria prophylaxis and liver-stage eradication. In this paper, new coumarin-based triclosan analogues are reported and their biological profile is explored in terms of inhibitory potency against enzymes of the *Pf*FAS-II pathway. Among the tested compounds, **7** and **8** showed the highest inhibitory potency against *Pf* enoyl-ACP-reductase (*Pf*FabI), followed by **15** and **3**. Finally, we determined the crystal structures of compounds **7** and **11** in complex with *Pf*FabI to identify their mode of binding and to confirm outcomes of docking simulations.

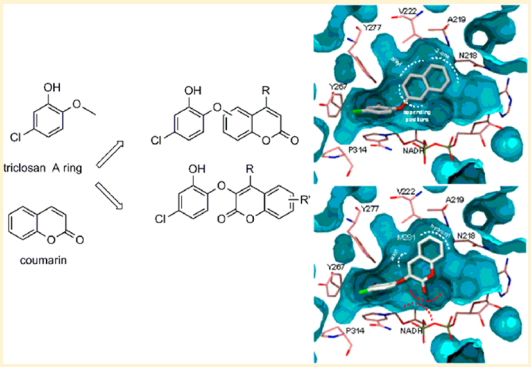

INTRODUCTION

Malaria, caused by protozoan parasites of the genus *Plasmodium*, is one of the most widespread and devastating infectious tropical diseases, killing more than one million people each year and continuously undermining the economic development opportunities of countries in the tropical and subtropical zones of the world.[1] The current emergence and spread of chloroquine-resistant *Plasmodium falciparum* (*Pf*) strains represent major obstacles for the control of the disease, impairing both prophylaxis and chemotherapy. Even worse, the first signs of resistance to artemisinin, the newest and most effective antimalarial drug currently available, were identified in Cambodia in 2006, and the resistance has now spread along the border with Thailand.[2] Although attempts to develop a vaccine for malaria are ongoing, drugs continue to be the only treatment option.[3] Consequently, there is an urgent need to develop potent and safe antimalarial drugs.

The *Plasmodium* life cycle in the mammalian host begins with sporozoites in the saliva of a female *Anopheles* mosquito, which are injected into the dermis of the human host during the blood meal. After migration to the liver, the sporozoites invade and infect hepatocytes leading to the liver stage (LS) of the parasite life cycle.[4−6] During this stage, which is clinically silent, the sporozoites grow and undergo replication, culminating in the release of tens of thousands of merozoites into the bloodstream to invade erythrocytes for subsequent asexual propagation. This so-called blood stage (BS) is responsible for most of the malaria symptoms. In *P. vivax* and *P. ovale*, a number of LS parasites remain in the hepatocytes as a dormant form (hypnozoite), which is difficult to eradicate and can lead to recurrent infections even after months or years.[7]

With the exception of primaquine, the currently available antimalarial drugs are blood schizontocidals targeting the pathogenic, asexual BS parasites.[8] However, full inhibition of the parasite development during the obligatory LS would lead to true causal prophylaxis, thus preventing pathology or at least decreasing the severity of the disease. Furthermore, the low

Received: January 6, 2013

   dx.doi.org/10.1021/jm400637m | *J. Med. Chem.* XXXX, XXX, XXX−XXX

number of hepatic forms substantially reduces the likelihood of selecting for drug-resistant parasites. Transmission would also be interrupted because it depends on gametocytes that mature in red blood cells.[9] Thus, agents directed to the LS constitute a promising strategy for malaria prophylaxis and eradication and are likely to be beneficial for high-risk groups (e.g., children and pregnant women) living in malaria endemic areas or travelers exposed to the disease while visiting those areas. To achieve the goal of malaria eradication, drug discovery efforts must continue to produce new drugs, targeted at unconventional vital parasite functions, such as new metabolic pathways.

Recent transcriptomic and proteomic findings on *Plasmodium* parasites in isolated LS hepatocytes revealed protein classes and metabolic pathways that have the potential to serve as drug targets for malaria prophylaxis.[10] Among others, several enzymes involved in fatty acid synthesis, including those of the *Pf* type II fatty acid biosynthesis (*Pf*FAS-II) pathway, are overrepresented in the LS parasites.[10] This is well in line with the recent discovery that the *Pf*FAS-II pathway is essential for correct LS development,[11,12] although it was previously considered to function only in the BS parasite.[13,14] The inherent differences between the fatty acid biosynthesis pathway of the parasite (FAS-II) and that of the human host (FAS-I) offer a great opportunity to develop highly specific antimalarial agents.[11,12]

Fatty acids are produced via enzymatic steps consisting of repeated cycles of elongation reactions, each including condensation, dehydration, and reduction. The growing acyl substrate is covalently bound to the acyl carrier protein (ACP), which shuttles and delivers the substrate from one enzyme to the other.[15] The FAS-II pathway is composed of a series of distinct and highly conserved enzymes, among which are β-ketoacyl-ACP-reductase (FabG), β-hydroxacyl-ACP-dehydratase (FabZ), and enoyl-ACP-reductase (FabI, also known as ENR). FabI, responsible for the concluding reduction step of each elongation cycle, represents a key physiological regulator of fatty acid biosynthesis and has been validated as an important drug target for the development of antibacterials[16] and antimalarials.[17,18] FabI is a key enzyme that is responsible for the NADH-dependent reduction of *trans*-2-enoyl-ACP to saturated acyl-ACP, and its three-dimensional structure in complex with several inhibitors has been characterized by X-ray crystallography.[19]

Among the inhibitors reported in the literature, triclosan, 5-chloro-2-(2,4-dichlorophenoxy)phenol (compound **1**, Figure 1),

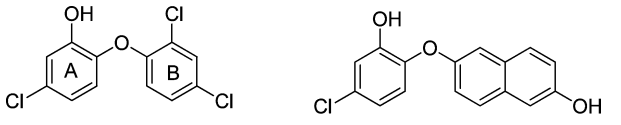

Figure 1. *Pf*FabI inhibitors **1** and **2**.

is considered to be a prototypical lead compound that specifically inhibits FabI in several species. In particular, triclosan has been reported to act against a broad spectrum of bacteria,[20] including *Escherichia coli*,[21] *Mycobacterium tuberculosis*,[22] multidrug-resistant *Staphylococcus aureus*,[23] but also the unicellular parasite *P. falciparum*.[24] Triclosan inhibits *P. falciparum* with an IC_{50} of around 1 μM [19,24,25] and exhibits a K_i of 50 nM against purified *P. falciparum* FabI (*Pf*FabI).[19] The structural basis of *Pf*FabI in complex with **1** has been elucidated and allowed the identification of structural features important for *Pf*FabI inhibition. In particular, the 2-hydroxy-4-chlorophenyl fragment of **1** (called ring A) plays a fundamental role in binding affinity, since both the aryl moiety and its functional groups, together with the cofactor NADH, are involved in several noncovalent interactions with the side chains of amino acid residues. In particular, the hydroxyl group and the ether oxygen linking the two aromatic rings are critical for binding.[19] When the 2′,4′-dichlorophenyl moiety (called ring B) of **1** was replaced with an extended naphthalene function bearing a hydroxyl group (**2**, Figure 1), three new hydrogen bonds could be established via the additional hydroxyl moiety.[19] On the basis of these findings, drug discovery projects have largely focused on analogues of **1**, affording a large collection of diaryl ethers with strong activity toward the parasite or the target enzyme.[19,26−28]

The present study reports on the design and synthesis of novel analogues of **1** obtained by replacing its B ring with a coumarin moiety, which represents a naturally occurring scaffold found in several marketed drugs. The molecules were then tested using biochemical and cell-based assays to assess their antiplasmodial profile. Docking simulations supported the design strategy, and the X-ray cocrystal structures of compounds **7** and **11** in complex with *Pf*FabI were solved to disclose the binding mode. The promising results point to these new chemical entities as potential hit compounds for discovering novel antimalarial compounds to be utilized as effective agents for malaria prophylaxis.

RESULTS AND DISCUSSION

Design Strategy. Coumarins, a class of compounds found widely in nature, show a broad spectrum of activities and are frequently associated with low toxicity.[29] Because of their inherent affinity for several biological targets, coumarins can be regarded as a privileged scaffold and represent an ideal framework for the design of compounds able to interact with different targets.[30] Our strategy was to link the 2-hydroxy-4-chlorophenyl of **1** (ring A) to selected coumarin backbones to afford a new druglike scaffold, which has the potential to engage in new interactions with the target and enable further exploration of the *Pf*FabI active site. The design of the compounds was carried out by taking advantage of the available crystal structures of *Pf*FabI in complex with **1** and derivatives thereof[19] and was supported by docking simulations. We designed two series of molecules (Tables 1 and 2), hereafter referred to as series I (**3**−**8**) and series II (**9**−**15**).

Docking of both series showed that we could replace the lipophilic subunit of **1** with a chromenone function while keeping relevant interactions within the *Pf*FabI active site. Figure 2 shows a schematic representation of docking of series I (Figure 2A) and II (Figure 2B). In these models, ring A engages a stacking interaction with the nicotinamide ring of NADH, with hydrogen bonds to the 2′-hydroxyl group of the nicotinamide ribose and with Tyr277. The 4-chloro atom of ring A was surrounded by hydrophobic residues and made van der Waals contacts with the side chains of Tyr267, Pro314, and Phe368. The coumarin moiety occupied the same pocket of ring B as **1**, lying on the side chain of Met281 and suggesting a possible sulfur−arene interaction.[31]

Docking solutions for compounds **3** and **6**, in which the A ring was inserted on positions 6 and 7 of the coumarin scaffold, clustered in an almost identical fashion, maintaining the native interactions of the A ring of **1** and suggesting a good shape-complementarity between the coumarin portion and the binding site. Furthermore, the coumarin-2-one function could form H-bonds with both the backbone nitrogen of Ala219 and the side chain of Asn218 (Figure 2A).

dx.doi.org/10.1021/jm400637m | J. Med. Chem. XXXX, XXX, XXX−XXX

Table 1. Inhibitory Activities of Series I (Compounds 3−8) and Reference Compounds: IC_{50} (μM) for *Pf*FAS-II Enzymes from *P. falciparum* and in Vitro Antiplasmodial Activities against Drug Resistant *P. falciparum* K1 Strain and Activity on Mammalian L6 Cells (Cytotoxicity) (μM)[a]

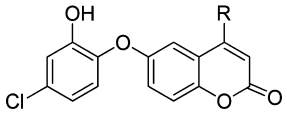

3-5: insertion position 6

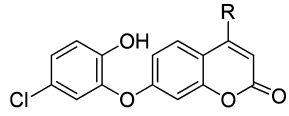

6-8: insertion position 7

compd	R	*Pf*FabI	*Pf*FabG	*Pf*FabZ	*Pf*K1[b]	L-6	SI[c]
3	H	0.63	nd	nd	10.7	96.2	9.0
4	CH_3	14.2	nd	nd	15.6	35.5	2.2
5	CH_2CH_3	11.0	nd	nd	5.6	142.0	25.6
6	H	2.7	nd	nd	9.3	187.6	20.1
7	CH_3	0.25	>100	>100	9.5	85.9	9.0
8	CH_2CH_3	0.27	>100	>100	5.7	84.8	14.9
triclosan (**1**)[d]		0.05			1.51		
(−)-epigallocatechin gallate			0.32	0.03			
chloroquine					0.23		
podophyllotoxin						0.006	

[a]IC_{50} values represent the concentration of a compound that causes 50% growth inhibition and are the mean of three independent experiments for the enzyme inhibition assay and are the average of at least two independent assays performed in duplicate for the cell assay. The errors for individual measurements differed by less than 50%. [b]Resistant to chloroquine and pyrimethamine. [c]SI = IC_{50}(L-6)/IC_{50}(parasite). [d]See ref 43.

Table 2. Inhibitory Activities of Series II (Compounds 9−15) and Reference Compounds: IC_{50} (μM) for *Pf*FAS-II Enzymes from *P. falciparum* and in Vitro Antiplasmodial Activity against Drug Resistant *P. falciparum* K1 Strain and Activity on Mammalian L6 Cells (Cytotoxicity) (μM)[a]

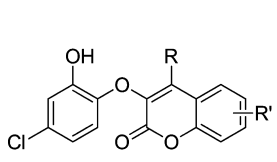

9-14

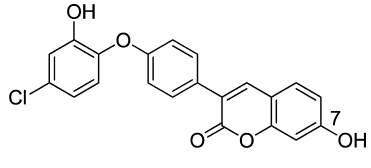

15

compd	R	R′	*Pf*FabI	*Pf*FabG	*Pf*FabZ	*Pf*K1[b]	L-6	SI[c]
9	H	H	5.5	>100	>100	15.0	108.4	7.2
10	H	6-OH	14.0	>100	>100	>15.0	134.2	>9.5
11	H	7-OH	6.0	99	16.3	>15.0	143.9	>9.6
12	H	5,7-di-OH	44	>100	90	>15.0	127.9	>8.5
13	CH_3	H	12.0	>100	13	>15.0	51.53	>3.4
14	CH_3	7-OH	15.0	>100	28	>15.0	96.3	>6.4
15			0.45	>100	10	8.0	41.0	5.1
triclosan (**1**)[d]			0.05			1.51		
(−)-epigallocatechin gallate				0.32	0.03			
chloroquine						0.23		
podophyllotoxin							0.006	

[a]IC_{50} values represent the concentration of a compound that causes 50% growth inhibition and are the mean of three independent experiments for the enzyme inhibition assay and are the average of at least two independent assays performed in duplicate for the cell assay. The errors for individual measurements differed by less than 50%. [b]Resistant to chloroquine and pyrimethamine. [c]SI = IC_{50}(L-6)/IC_{50}(parasite). [d]See ref 43.

A relatively small and hydrophobic pocket formed by the side chain of residues Val222, Tyr267, Met281, and Ile323 and adjacent to position 4 of the coumarin moiety (Figure 2A) suggested the possibility of introducing 4-methyl and 4-ethyl substituents at this position (**4**, **5**, **7**, **8**). Docking of **7** and **8** generated a single cluster of poses with the 4-substituents inserted into this hydrophobic pocket, thus providing an additional anchoring point within the binding site. Hydroxylated derivatives were finally designed to explore the possibility of establishing new H-bonds. The high score obtained with 7-monohydroxylated ligands (**11**, **12**, **14**) suggested a possible network of H-bonds with the side chain nitrogen of Asn218 and the main chain oxygen and nitrogen of Ala219.

Compounds **3**−**15** were then synthesized and biologically tested to assess their antimalarial profile, namely, inhibitory activity against multiple *Pf*FAS-II elongation enzymes (*Pf*FabI, *Pf*FabZ, and *Pf*FabG) and in vitro growth inhibitory potential against malaria parasites (drug resistant *P. falciparum* K1 strain). Furthermore, their toxicity against mammalian cells was assessed against a primary cell line derived from rat skeletal myoblasts (L6).

Chemistry. The Ullmann-type copper-catalyzed coupling of brominated coumarin intermediates **16**−**21** and **34** with

dx.doi.org/10.1021/jm400637m | J. Med. Chem. XXXX, XXX, XXX−XXX

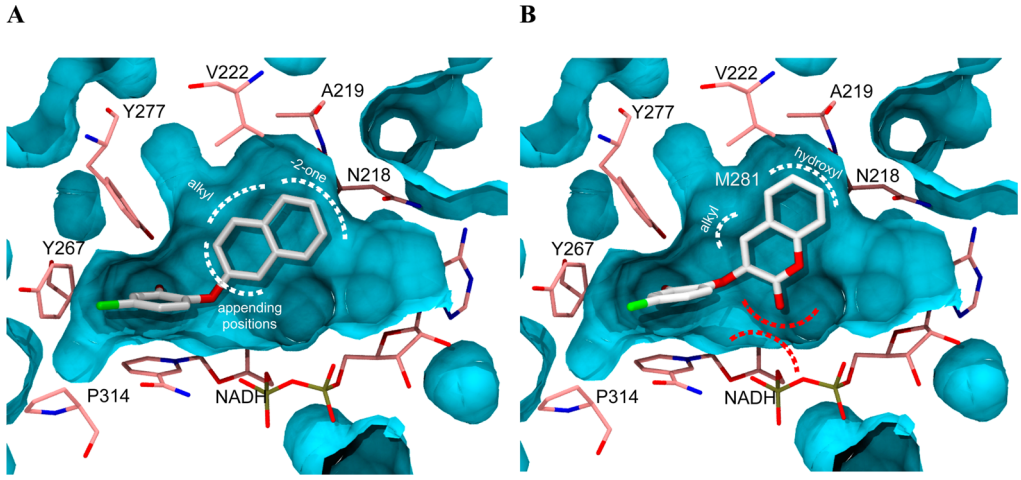

Figure 2. (A) Schematic representation of the backbone of compounds **3**–**8** (carbon atoms are white). The various substitutions, in which the A ring was appended on the aryl ring of the coumarin scaffold, are labeled. (B) Predicted binding mode for **9**–**14** (carbon atoms in white). Several substituents on the coumarin moiety were introduced and virtually tested for complementarity with the *Pf*FabI binding site (carbon atoms in pink). A section of the Connolly surface of the receptor is shown in blue.

Scheme 1. Synthesis of Series I *Pf*FabI Inhibitors (3–8)[a]

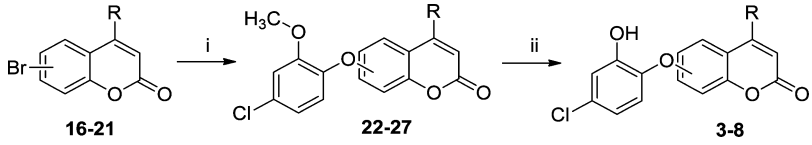

[a]Reagents and conditions: (i) 4-chloro-2-methoxyphenol, Cs_2CO_3, (CuOTf)·PhH, ethyl acetate, 1-naphthoic acid, activated 5 Å molecular sieves, toluene, 110 °C, N_2; (ii) BBr_3, DCM, −70 °C, N_2 atmosphere.

Scheme 2. Synthesis of Series II *Pf*FabI Inhibitors (9–14)[a]

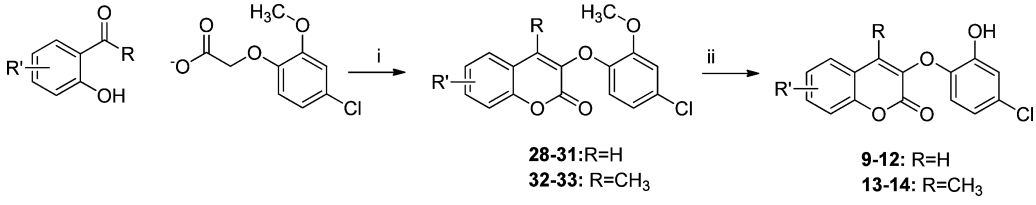

[a]Reagents and conditions: (i) triethylamine, Ac_2O, 180 °C; (ii) BBr_3, DCM, −70 °C, N_2 atmosphere.

Scheme 3. Synthesis of *Pf*FabI Inhibitor 15[a]

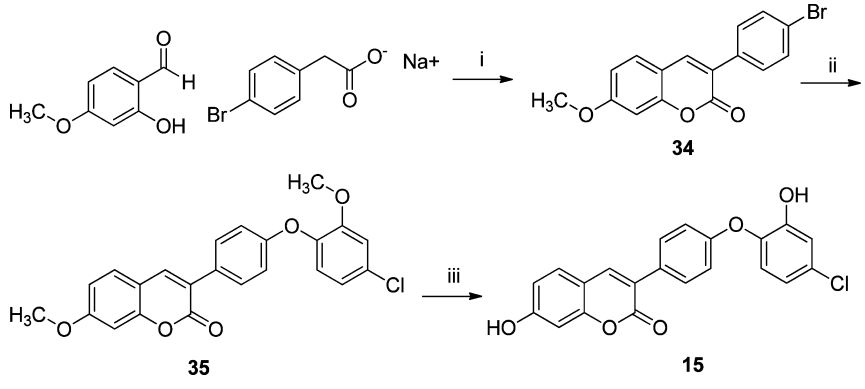

[a]Reagents and conditions: (i) triethylamine, Ac_2O, 180 °C; (ii) 4-chloro-2-methoxyphenol, Cs_2CO_3, (CuOTf)·PhH, ethyl acetate, 1-naphthoic acid, activated 5 Å molecular sieves, toluene, 110 °C, N_2 atmosphere; (iii) BBr_3, DCM, −70 °C, N_2.

4-chloro-2-methoxyphenol gave the desired diaryl ethers **22**–**27** and **35** (Schemes 1 and 3, respectively). Different synthetic strategies were employed to obtain the suitable brominated coumarin intermediates (**16**–**21**) (see the Experimental Section). Compound **34** was obtained according to Scheme 3, in which the 2-hydroxy-4-methoxybenzaldehyde was reacted

dx.doi.org/10.1021/jm400637m | J. Med. Chem. XXXX, XXX, XXX–XXX

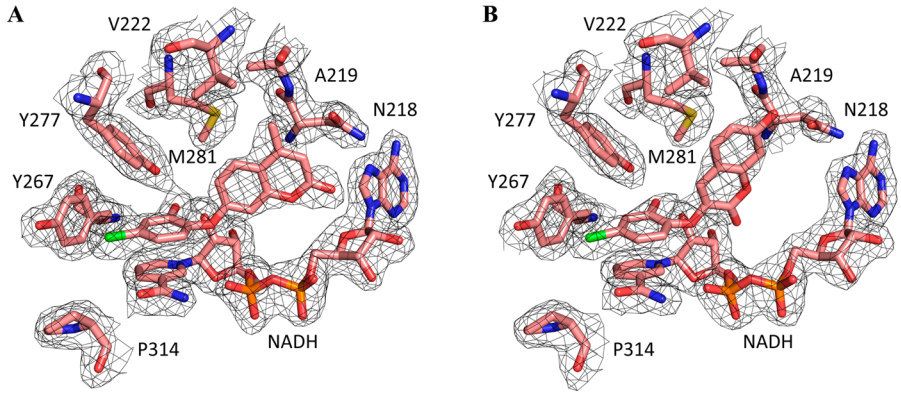

Figure 3. View of the $2mF_o - DF_c$ electron density map contoured at 1.0σ for bound analogues **7** (A) and **11** (B) and cofactor NADH.

with sodium 2-(4-bromophenyl)acetate in the presence of triethylamine. Similarly, **28**−**33** (Scheme 2) were prepared by reaction of suitable methoxylated 2-hydroxybenzaldehyde and 2-hydroxyacetophenone with sodium 2-(4-chloro-2-methoxyphenoxy)acetate. The methoxy groups were removed by treatment with BBr_3 to afford the final compounds as phenol derivatives (**3**−**15**).

Inhibition of *Pf*FabI. The ability of **3**−**15** to inhibit the recombinant *Pf*FabI enzyme was investigated by using a spectrophotometric assay (see the Experimental Section for details). All data are shown in Tables 1 and 2. Compounds **3**−**8**, where ring A of **1** is attached to either the 6- or 7-position of the coumarin scaffold, inhibited *Pf*FabI with IC_{50} values in the low micromolar to the submicromolar range. Among them, **6** exhibited moderate *Pf*FabI inhibition (IC_{50} = 2.7 μM), while **7** and **8**, obtained by appending the A ring of **1** at the 7-position of a 4-alkylcoumarin scaffold, showed the highest inhibitory activity with IC_{50} values of 0.25 and 0.27 μM, respectively. A different trend was observed for the 6-subtituted subset of compounds (**3**−**5**). Derivative **3**, bearing an unsubstituted coumarin subunit, showed a strong inhibitory effect against *Pf*FabI, with an IC_{50} value of 0.63 μM, while the inhibition was decreased in the 4-alkylcoumarin analogues **4** and **5** relative to **3**.

With series II (**9**−**15**), we explored linking the A ring of **1** to position 3 of several different coumarins. All compounds in this subset displayed moderate activity toward *Pf*FabI (micromolar to low-micromolar IC_{50} values), with the exception of **15** featuring a 3-arylcoumarin subunit, which turned out to be the most active compound within series II (IC_{50} = 0.45 μM).

Derivative **9** and the 7-hydroxylated analogue **11** inhibited *Pf*FabI with IC_{50} values of 5.5 and 6.0 μM, respectively, and potency was further reduced in the 6-hydroxy derivative (**10**, IC_{50} = 14.0 μM) and in the 5,7-dihydroxy disubstituted analogue **12** (IC_{50} = 44.0 μM). The introduction of a 4-methyl group in **9** and **11**, affording compounds **13** and **14**, respectively, caused a 2-fold reduction in the activity compared to the parent compounds. Conversely, a remarkable improvement in potency was obtained by inserting a bridging phenyl group between position 3 of the 7-hydroxycoumarin scaffold and the A ring of **1** (compound **15**), lowering the IC_{50} value by 1 order of magnitude with respect to the close analogue **11**.

Inhibition of *Pf*FabG and *Pf*FabZ. To analyze selectivity with respect to other enzymes involved in parasite fatty acid biosynthesis pathway, we tested a selection of the new molecules (**7**−**15**) against *Pf*FabZ and *Pf*FabG, two enzymes also belonging to the chain elongation cycle of pathway. Data are reported in Tables 1 and 2. All compounds were inactive against *Pf*FabG (IC_{50} > 100 μM), whereas **11**−**15** were able to moderately inhibit *Pf*FabZ. The latter compounds are therefore dual *Pf*FabI/*Pf*FabZ inhibitors, targeting two enzymes in the same pathway.

Antimalarial Activity against Multidrug Resistant *P. falciparum*. The in vitro antiplasmodial activity of the designed coumarin-based triclosan analogues (**3**−**15**) against multidrug resistant *P. falciparum* K1 strain was determined by using the established ^{3}H-hypoxanthine method (see the Experimental Section for details). As shown in Tables 1 and 2, the antimalarial potential of compounds **3**−**8** and **15**, endowed with the entire diaryl ether function, proved to be substantially superior with respect to compounds **9**−**14** of series II. Among series I, derivatives **5** and **8** showed a good activity against the malaria parasite (IC_{50} values of 5.6 and 5.7 μM, respectively). A common chemical feature of these compounds is an ethyl substituent in position 4 of the coumarin scaffold. The other compounds of the series (i.e., **3**, **6**, **7**, and **15**) showed a moderate decrease in potency with respect to the former ones. A further decrease in antiplasmodial activity was observed for series II (compounds **9**−**14**) whose IC_{50} values were superior to 15 μM.

The low activity of the compounds on BS parasites was not fully unexpected. Indeed, FAS-II is only moderately active in BS parasites, and therefore, the activities of **3**−**9** could also be due to activity against other targets not belonging to the FAS-II pathway. However, the aim of these experiments was to test the ability of these molecules to act at an intracellular level, and further experiments using the LS parasites will be conducted to fully characterize the biological profile of this new series of antimalarial compounds.

As a positive feature, all compounds showed low cytotoxicity on mammalian cells (L6), indicating that the selected coumarin scaffold, upon the designed functionalization, did not elicit toxic effect. The compounds selectivity index (SI) was calculated as the ratio of cell growth inhibition (IC_{50} values) for mammalian cells to that for the selected parasite, according to the WHO/TDR guidelines (see footnote c in the tables for detailed formula).

Crystal Structures of *Pf*FabI in Complex with 7 and 11. To investigate the binding mode at an atomic level, we solved the structures of *Pf*FabI in complex with **7** (series I, PBD code 4IGE, Figure 3A) and **11** (series II, PDB code 4IGF, Figure 3B), following the protocol previously reported by Perozzo et al.[19] The corresponding crystallographic data and refinement statistics may be found in the Supporting Information (Table S1).

Comparison of the structures reported in this study with those previously published[19] revealed no major structural differences. The overall protein and the active site residues were in the very

dx.doi.org/10.1021/jm400637m | J. Med. Chem. XXXX, XXX, XXX−XXX

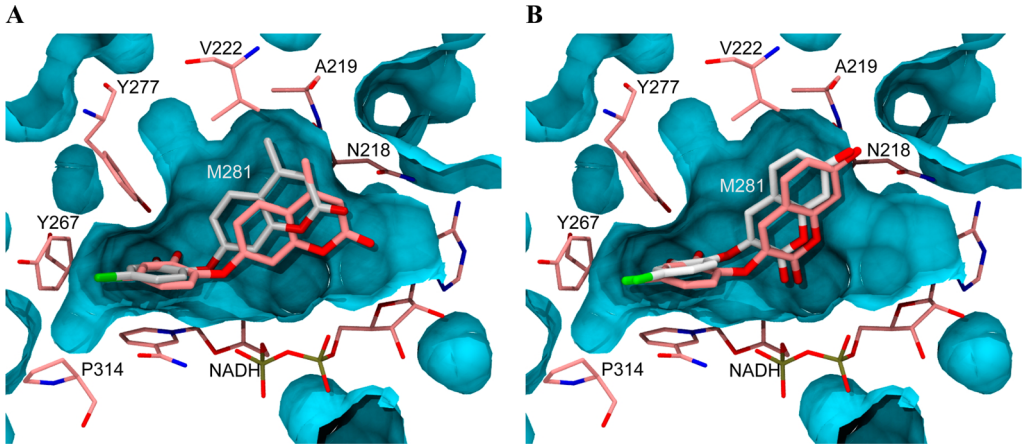

Figure 4. Comparison between the predicted binding mode (carbon atoms in gray) and the experimentally determined binding mode (carbon atoms in pink) for **7** (A) and **11** (B) in complex with *Pf*FabI and NADH. The RMSD calculated between the docking model and the crystal structure using non-hydrogen atoms of **7** and **11** is 1.49 and 1.02 Å, respectively. A section of the Connolly surface of the receptor is shown in blue.

same position, highlighting a high degree of conservation between the present and the previously reported crystallographic structures (see Figures 1 and 2 in the Supporting Information). In both complexes, the position of the cofactor NADH was clearly defined by excellent electron density, showing NADH binding in the typical extended conformation with both ribose sugar rings in the C2′-*endo* conformation and the nicotinamide group in the *syn* conformation.

The crystal structures of *Pf*FabI in complex with **7** and **11** unambiguously revealed the binding mode of the inhibitors showing strong and continuous difference density for **7** (Figure 3A) in both monomers and for **11** in monomer B (Figure 3B). Comparison of both structures with those of *Pf*FabI in complex with **1** and **2**[19] revealed that the binding mode was very similar, showing the same stacking interaction of ring A with the nicotinamide ring of NADH and the same hydrogen bonding pattern as observed in other structures, i.e., the phenolic hydroxyl hydrogen bonded to the 2′-hydroxyl moiety of the nicotinamide ribose and the oxygen atom of Tyr277 while van der Waals interactions were formed via the side chains of Tyr267, Tyr277, Pro314, Phe368, and Ile369. The ether oxygen atom of both compounds interacted with the 2′-hydroxyl group of the nicotinamide ribose at a distance of around 3.3 Å.

The coumarin ring systems of **7** and **11** were located in a pocket formed by the pyrophosphate and the nicotinamide group of NADH, the peptide backbone residues 217−231, and the side chains of Asn218, Val222, Tyr277, Met281, Ala319, and Ile323. Both coumarin moieties were oriented in a very similar way as observed for the extended ring B of **2**, tilted by about 10° out of the plane found for ring B of **1**. This allowed **7** to interact with the backbone oxygen of Ala217 by H-bonding the ring oxygen in the coumarin group. Interestingly, the methyl substituent of the coumarin scaffold in **7** was predicted to fill the small and hydrophobic pocket located next to position 4 of the coumarin moiety, which is formed by the side chain of residues of Val222, Tyr267, Met281, and Ile323, implying a small rotation of the whole molecule toward this pocket. However, this movement did not occur, as **7** maintained the conserved binding mode with the methyl group only pointing to the pocket but not filling it. This is probably due to the penalizing effect of losing the H-bond formed between Ala217 and the coumarin group. As observed for **2**, compound **11** could also establish the same three H-bonds through the hydroxyl group of the coumarin ring, the side chain nitrogen of Asn218, and the main chain oxygen and nitrogen of A219. Moreover, the ring oxygen in the coumarin group of **11** could also interact with the backbone oxygen of Ala217.

The docking binding mode and the pool of interactions predicted for compounds **7** and **11** were confirmed and found to be in good agreement with those detected in the crystal structure of the ternary complex with *Pf*FabI and NADH (Figure 4A and Figure 4B, respectively). In particular, after superimposition of the protein backbone, we observed that **7** showed an RMSD of 1.49 Å between the docking model and the crystal structure (Figure 4A), while the RMSD was 1.02 Å for the docking model of **11** vs the experimentally determined binding mode (Figure 4B).

CONCLUSIONS

In this study, the introduction of ring A of **1** to purposely selected positions of a coumarin scaffold led to a new series of *Pf*FabI inhibitors that could be regarded as tools to explore the chemical space of the target. Compounds of series I (**3**−**8**), together with **15**, gave the best results in terms of both inhibition of *Pf*FabI enzyme and antiplasmodial actvity. In particular, derivatives **3**, **7**, **8**, and **15**, with submicromolar IC_{50} values, showed the highest potency against *Pf*FabI by virtue of the well-established capability of the diaryl ether function to interact with this enzyme. These compounds also showed micromolar IC_{50} values for inhibition of *P. falciparum* growth in the whole cell assays. From the data obtained, some conclusions can be drawn: (i) the presence of a 2-hydroxy-4-chlorophenyl-based diaryl ether framework, as a capping fragment, plays a fundamental role in the inhibition of both *Pf*FabI and parasite growth; (ii) the coumarin scaffold is tolerated by *Pf*FabI.

X-ray data suggested that potency toward *Pf*FabI resulted from interactions between the enzyme active site and two separate parts of the coumarin framework, such as the 2-one function and the substituent at position 4 of the coumarin scaffold. In particular, the coumarin-2-one function was responsible for a penalizing orientation toward the pyrophosphate moiety of NADH (compounds **9**−**14**) and was able to interact favorably with nitrogen of Ala219 backbone and the side chain of Asn218 (compounds **3**−**8**). An improvement in potency was achieved by introducing an alkyl substituent at position 4 of the main backbone, thus providing an additional anchoring point within the binding site.

dx.doi.org/10.1021/jm400637m | *J. Med. Chem.* XXXX, XXX, XXX−XXX

These encouraging results allow us to consider this new class of coumarin-based triclosan analogues as a promising starting point for a drug discovery program aimed at exploring in more depth the significance of the coumarin framework for interaction with FabI from *P. falciparum*. For instance, compound **8** is a promising hit because of its *Pf*FabI inhibitory activity (IC_{50} = 0.27 μM), selectivity vs *Pf*FabG and *Pf*FabZ, and antiplasmodial activity (IC_{50} = 5.7 μM), which is only 4- to 5-fold less than that of **1**. Derivatives **7** and **15** also exhibited substantial antimalarial activity. In particular, compound **15**, because of its unique structure, may represent a promising starting point for lead optimization.

Finally, FabI enzymes are widely and intensively investigated as potential antibacterial targets. Because of the high sequence homology between *Plasmodium* and bacterial isoforms, the inhibitors presented herein could also be relevant in the field of antibacterial drug discovery.[6]

EXPERIMENTAL SECTION

Chemistry. General Procedures. Starting materials, unless otherwise specified in the Experimental Section, were used as high-grade commercial products. Solvents were of analytical grade. Melting points were determined in open glass capillaries, using a Büchi apparatus, and are uncorrected. ^{1}H NMR and ^{13}C NMR spectra were recorded on Varian Gemini spectrometers at 200, 300, or 400 MHz, and chemical shifts are reported in parts per million (ppm δ value) relative to the peak for tetramethylsilane (TMS) as internal standard. Standard abbreviations indicating spin multiplicities are given as follows: s (singlet), d (doublet), t (triplet), br (broad), q (quartet), or m (multiplet). Mass spectra were recorded on a Waters ZQ 4000 apparatus operating in electrospray mode (ES). Wherever analyses are only indicated with element symbols, analytical results obtained for those elements are within 0.4% of the theoretical values. Chromatographic separations were performed on silica gel columns using the flash method (Kieselgel 40, 0.040−0.063 mm, Merck). Reactions were followed by thin layer chromatography (TLC) on precoated silica gel plates (Merck silica gel 60 F254) and then visualized with a UV lamp. Satisfactory elemental analyses were obtained for all new compounds, confirming >95% purity. Compounds were named following IUPAC rules as applied by Beilstein-Institute AutoNom (version 2.1), a PC-integrated software package for systematic names in organic chemistry.

6-Bromo-2*H*-chromen-2-one (16). A mixture of 5-bromo-2-hydroxybenzaldehyde (3.0 g, 14.9 mmol) and sodium acetate (1.22 g, 14.9 mmol) in acetic anhydride (2.82 mL, 29.8 mmol) was heated at 180 °C for 8 h. When the mixture was cooled, a 10% K_2CO_3 aqueous solution was added, and the solid residue was filtered and crystallized from ligroin to obtain compound **16** as yellowish needles (1.9 g, 56% yield), mp 166−168 °C. ^{1}H NMR ($CDCl_3$, 200 MHz): δ 6.47 (d, J = 9.6 Hz, 1H), 7.22 (dd, J = 2.2 and 8.4 Hz, 1H), 7.24 (d, J = 2.2 Hz, 1H), 7.62 (d, J = 8.4 Hz, 1H), 7.66 (d, J = 9.6 Hz, 1H). MS (ESI$^+$) m/z: 225 [M + H]$^+$. Exact mass: 223.9473.

6-Bromo-4-methyl-2*H*-chromen-2-one (17). Following the procedure described for **16**, starting from 1-(5-bromo-2-hydroxyphenyl)ethanone (4.10 g, 19.06 mmol), compound **17** was obtained as colorless needles (2.20 g, 50% yield), mp 190−192 °C. ^{1}H NMR ($CDCl_3$, 200 MHz): δ 2.43 (s, 3H), 6.33 (s, 1H), 7.20 (d, J = 8.8 Hz, 1H), 7.60 (dd, J = 2.2 and 8.8 Hz, 1H), 7.72 (d, J = 2.2 Hz, 1H). MS (ESI$^+$) m/z: 239 [M + H]$^+$. Exact mass: 237.9629.

6-Bromo-4-ethyl-2*H*-chromen-2-one (18). A solution of 1-(5-bromo-2-hydroxyphenyl)propan-1-one (1 g, 4.4 mmol) and methyl (triphenylphosphoranylidene)acetate (2.3 g, 6.6 mmol), in benzene (10 mL), was heated under reflux for 24 h. The solvent was removed under reduced pressure and the crude product was purified by flash column chromatography using a mixture of petroleum ether/ethyl acetate (90:10) as eluent to afford **18** (2.1 g, 60% yield), mp 115−117 °C. ^{1}H NMR ($CDCl_3$, 200 MHz): δ 1.34 (t, J = 7.8 Hz, 3H), 2.79 (q, J = 7.8 Hz, 2H), 6.33 (s, 1H), 7.24 (d, J = 8.8 Hz, 1H), 7.60 (dd, J = 2.2 and 8.8 Hz, 1H), 7.75 (d, J = 2.2 Hz, 1H). MS (ESI$^+$) m/z: 253 [M + H]$^+$. Exact mass: 251.9786.

7-Bromo-2*H*-chromen-2-one (19). To a mixture of 3-bromophenol (1 g, 5.8 mmol) and malic acid (0.52 g, 3.9 mmol) at 0 °C was added dropwise 98% H_2SO_4 (1.3 mL), and the resulting solution was heated at 120 °C for 6 h. After the mixture was cooled to room temperature, crushed ice was added, and the precipitated solid was collected by filtration. Purification by crystallization from ethanol gave the desired compound **19** as a white solid (0.80 g, 80% yield), mp 121−123 °C. ^{1}H NMR ($CDCl_3$, 200 MHz): δ 6.39 (d, J = 9.6 Hz, 1H), 7.11 (dd, J = 8.4 and 1.8 Hz, 1H), 7.15 (d, J = 1.8 Hz, 1H), 7.43 (d, J = 8.4 Hz, 1H), 7.55 (d, J = 9.6 Hz, 1H). MS (ESI$^+$) m/z: 225 [M + H]$^+$. Exact mass: 223.9473.

7-Bromo-4-methyl-2*H*-chromen-2-one (20). To a solution of 3-bromophenol (1 g, 5.81 mmol), ethyl 3-oxobutanoate (0.74 mL, 5.80 mmol), and ethyl alcohol (58 mL) at 0 °C was added dropwise a 70% H_2SO_4 aqueous solution (0.62 mL, 11.6 mmol). The resulting solution was stirred at room temperature overnight and then poured into crushed ice. The solid formed was filtered and crystallized from toluene to afford **20** as a white solid (0.90 g, 90% yield), mp 118−120 °C. ^{1}H NMR ($CDCl_3$, 200 MHz): δ 2.52 (s, 3H), 6.32 (s, 1H), 7.01−7.15 (m, 1H), 7.23 (s, 1H), 7.45 (dd, J = 2.1 and 8.4 Hz, 1H). MS (ESI$^+$) m/z: 239 [M + H]$^+$. Exact mass: 237.9629.

7-Bromo-4-ethyl-2*H*-chromen-2-one (21). Following the procedure described for **18**, starting from 1-(4-bromo-2-hydroxyphenyl)-propan-1-one (2.5 g, 10.9 mmol) and methyl(triphenylphosphoranylidene)acetate (5.69 g, 16.3 mmol) in benzene (15 mL), compound **21** was obtained as colorless needles (1.5 g, 54% yield), mp 130−132 °C. ^{1}H NMR ($CDCl_3$, 200 MHz): δ 1.33 (t, J = 7.6 Hz, 3H), 2.80 (q, J = 7.8 Hz, 2H), 6.31 (s, 1H), 7.44−7.51 (m, 3H). MS (ESI$^+$) m/z: 253 [M + H]$^+$. Exact mass: 251.9786.

3-(4-(4-Chloro-2-methoxyphenoxy)phenyl)-7-methoxy-2*H*-chromen-2-one (34). Following the procedure described for **16**, starting from 1-(2-hydroxy-4-methoxyphenyl)benzaldehyde (0.4 g, 2.7 mmol) and sodium 2-(4-bromophenyl)acetate (0.68 g, 2.7 mmol), compound **34** was obtained as a white solid (0.43 g, 48% yield), mp 184−187 °C. ^{1}H NMR ($CDCl_3$, 400 MHz): δ 3.90 (s, 3H), 6.86 (d, J = 2.0 Hz, 1H), 6.87 (dd, J = 2.0 and 8.4 Hz, 1H), 7.46 (d, J = 8.4 Hz, 1H), 7.50−7.59 (m, 4H), 7.77 (s, 1H). MS (ESI$^+$) m/z: 331 [M + H]$^+$. Exact mass: 329.9892.

Sodium 2-(4-Chloro-2-methoxyphenoxy)acetate. A solution of 4-chloro-2-methoxyphenol (0.6 g, 3.85 mmol), 2-chloroacetic acid (0.40 g, 4.2 mmol), K_2CO_3 (1.16 g, 8.47 mmol), and KI (0.10 g) in acetone (50 mL) was heated under reflux for 8 h. The solvent was removed under reduced pressure, and the solid was suspended in CH_2Cl_2 and washed with 2 N NaOH (2 × 20 mL) and then with brine (20 mL). The organic layer was dried over anhydrous Na_2SO_4 and concentrated to dryness to give the desired product (0.40 g, 90% yield), mp 126−132 °C. The compound was then transformed into the sodium salt by adding a 10% NaOH in ethyl alcohol (40 mL) and stirring at room temperature overnight. The solvent was removed under reduced pressure, and the white solid was dried (0.45 g, 95% yield). ^{1}H NMR (DMSO, 400 MHz): δ 3.85 (s, 3H), 4.05 (s, 2H), 6.70 (d, J = 8.4 Hz, 1H), 6.80 (dd, J = 8.4 and 1.8 Hz, 1H), 6.85 (d, J = 1.8 Hz, 1H).

General Procedure for the Synthesis of 3-(4-Chloro-2-methoxyphenoxy)-2*H*-chromen-2-one-Based Derivatives (28−33). A mixture of sodium 2-(4-chloro-2-methoxyphenoxy)acetate (0.60 g, 2.36 mmol), triethylamine (0.69 mL, 4.95 mmol) in acetic anhydride (0.60 g, 5.9 mmol), and the suitable 2-OH carbonyl compound (1.18 mmol) was heated at 180 °C for 8 h. When the mixture was cooled, a 10% K_2CO_3 aqueous solution was added, and the solution was extracted with CH_2Cl_2 (3 × 20 mL). The combined organic layers were dried over anhydrous Na_2SO_4 and concentrated to dryness to give a crude product that was purified by flash chromatography on silica gel, using a mixture of petroleum ether/ethyl acetate (80:10) as eluent.

3-(4-Chloro-2-methoxyphenoxy)-2*H*-chromen-2-one (28). Starting from 2-hydroxybenzaldehyde (0.14 g, 1.18 mmol), the desired derivative **28** was obtained (0.26 g, 72% yield), mp 136−138 °C. ^{1}H NMR ($CDCl_3$, 300 MHz): δ 3.80 (s, 3H), 6.40 (dd, J = 8.4 and 2.2 Hz, 1H), 6.80 (d, J = 2.2 Hz, 1H), 7.19 (d, J = 8.4 Hz, 1H), 7.20 (s, 1H),

dx.doi.org/10.1021/jm400637m | J. Med. Chem. XXXX, XXX, XXX−XXX

7.28−7.35 (m, 2H), 7.43−7.46 (m, 1H), 7.75 (d, J = 8.2 Hz, 1H). MS (ESI^+) m/z: 303/305 $[M + H]^+$. Exact mass: 302.0346.

3-(4-Chloro-2-methoxyphenoxy)-6-methoxy-2*H*-chromen-2-one (29). Starting from 2-hydroxy-5-methoxybenzaldehyde (0.36 g, 2.55 mmol), the desired derivative **29** was obtained (0.3 g, 36% yield), mp 135−138 °C. ^1H NMR ($CDCl_3$, 300 MHz): δ 3.78 (s, 3H), 3.80 (s, 3H), 6.65 (d, J = 2.2 Hz, 1H), 6.80 (dd, J = 2.2 and 8.4 Hz, 1H), 7.05 (d, J = 2.2 Hz, 1H), 7.09 (dd, J = 2.2 and 8.4 Hz, 1H), 7.12 (d, J = 2.2 Hz, 1H), 7.18 (d, J = 8.4 Hz, 1H), 7.30 (s, 1H). MS (ESI^+) m/z: 333/335 $[M + H]^+$. Exact mass: 332.0452.

3-(4-Chloro-2-methoxyphenoxy)-7-methoxy-2*H*-chromen-2-one (30). Starting from 2-hydroxy-4-methoxybenzaldehyde (0.58 g, 2.61 mmol), the desired derivative **30** was obtained (0.16 g, 74%, yield), mp 125−127 °C. ^1H NMR (CD_3COCD_3, 400 MHz): δ 3.83 (s, 3H), 3.93 (s, 3H), 6.93 (dd, J = 2.4 and 8.4 Hz, 1H), 7.08 (d, J = 2.4 Hz, 1H), 7.17 (s, 1H), 7.19 (d, J = 8.4 Hz, 1H), 7.36 (d, J = 1.8 Hz, 1H), 7.41 (dd, J = 1.8 and 8.2 Hz, 1H), 7.65 (d, J = 8.2 Hz, 1H). MS (ESI^+) m/z: 333/335 $[M + H]^+$. Exact mass: 332.0452.

3-(4-Chloro-2-methoxyphenoxy)-5,7-dimethoxy-2*H*-chromen-2-one (31). Starting from 2-hydroxy-4,6-dimethoxybenzaldehyde (1.07 g, 5.9 mmol), the desired derivative **31** was obtained (0.32 g, 14% yield), mp 129−130 °C. ^1H NMR ($CDCl_3$, 400 MHz): δ 3.81 (s, 3H), 3.85 (s, 3H), 3.88 (s, 3H), 6.41 (d, J = 2.2 Hz, 1H), 6.64 (d, J = 2.2 Hz, 1H), 6.90 (dd, J = 1.8 and 8.4 Hz, 1H), 7.0 (d, J = 8.4 Hz, 1H), 7.15 (d, J = 2.2 Hz, 1H), 7.25 (s,, 1H). MS (ESI^+) m/z: 363/365 $[M + H]^+$. Exact mass: 362.0557.

3-(4-Chloro-2-methoxyphenoxy)-4-methyl-2*H*-chromen-2-one (32). Starting from 1-(2-hydroxyphenyl)ethanone (0.13 mL, 0.98 mmol), the desired derivative **32** was obtained (0.15 g, 30% yield), mp 128−130 °C. ^1H NMR ($CDCl_3$, 300 MHz): δ 2.18 (s, 3H), 3.93 (s, 3H), 6.64 (dd, J = 1.8 and 8.4 Hz, 1H), 6.68 (dd, J = 1.8 and 8.4 Hz, 1H), 6.97 (d, J = 1.8 Hz, 1H), 7.26−7.39 (m, 2H), 7.53−7.55 (m, 1H), 7.65 (d, J = 8.4 Hz, 1H). MS (ESI^+) m/z: 317/319 $[M + H]^+$. Exact mass: 316.0502.

3-(4-Chloro-2-methoxyphenoxy)-7-methoxy-4-methyl-2*H*-chromen-2-one (33). Starting from 1-(2-hydroxy-4-methoxyphenyl)-ethanone (0.14 g, 0.81 mmol), the desired derivative **33** was obtained (0.07 g, 25% yield) mp 128−131 °C. ^1H NMR ($CDCl_3$, 300 MHz): δ 2.18 (s, 3H), 3.80 (s, 3H), 3.84 (s, 3H), 6.84 (d, J = 2.2 Hz, 1H), 6.88 (dd, J = 2.2 and 8.4 Hz, 1H), 7.06 (d, J = 2.2 Hz, 1H), 7.12 (dd, J = 2.2 and 8.4 Hz, 1H), 7.18 (d, J = 8.4 Hz, 1H), 7.45 (d, J = 8.4 Hz, 1H). MS (ESI^+) m/z: 347/349 $[M + H]^+$. Exact mass: 346.0608.

General Procedure for the Ulmann-Type Synthesis of Diaryl Ethers (22−27, 35).[32] In an oven-dried three-neck flask, a mixture of the bromocoumarin intermediate (2.5 mmol), 4-chloro-2-methoxyphenol (5.0 mmol), Cs_2CO_3 (5.0 mmol), (CuOTf)·PhH (0.0625 mmol, 5.0 mol % Cu), ethyl acetate (0.0125 mmol, 5.0 mol %), 1-naphthoic acid (5.0 mmol), and activated 5 Å molecular sieves (0.62 g) in toluene (2 mL) was heated at 110 °C under N_2 atmosphere for 24 h. When the mixture was cooled, 2 N NaOH (50 mL) was added and the aqueous layer was extracted with CH_2Cl_2 (3 × 50 mL). The combined organic layers were washed with brine, dried over anhydrous Na_2SO_4, and concentrated to dryness to give a crude product that was purified by flash chromatography on silica gel using a mixture of petroleum ether/ethyl acetate (90:10) as eluent.

6-(4-Chloro-2-methoxyphenoxy)-2*H*-chromen-2-one (22). Starting from **16** (0.6 g, 2.66 mmol), compound **22** was obtained (0.2 g, 24% yield), mp 143−146 °C. ^1H NMR ($CDCl_3$, 400 MHz): δ 3.81 (s, 3H), 6.42 (d, J = 9.6 Hz, 1H), 6.93 (dd, J = 1.8 and 8.4 Hz, 1H), 6.99 (d, J = 1.8 Hz, 1H), 7.00 (d, J = 8.4 Hz, 1H), 7.22 (dd, J = 1.8 and 8.4 Hz, 1H), 7.43 (d, J = 1.8 Hz, 1H), 7.45 (d, J = 8.4 Hz, 1H), 7.60 (d, J = 9.6 Hz, 1H). MS (ESI^+) m/z: 303/305 $[M + H]^+$. Exact mass: 302.0346.

6-(4-Chloro-2-methoxyphenoxy)-4-methyl-2*H*-chromen-2-one (23). Starting from **17** (0.58 g, 2.43 mmol), compound **23** was obtained (0.3 g, 39% yield), mp 120−122 °C. ^1H NMR ($CDCl_3$, 300 MHz): δ 2.37 (s, 3H), 3.78 (s, 3H), 6.12 (s, 1H), 6.93 (d, J = 2.2 Hz, 1H), 6.95 (dd, J = 2.2 and 8.4 Hz, 1H), 7.04 (d, J = 2.2 Hz, 1H), 7.11 (dd, J = 2.2 and 8.4 Hz, 1H), 7.19 (d, J = 8.4 Hz, 1H), 7.31 (d, J = 8.4 Hz, 1H). MS (ESI^+) m/z: 317/319 $[M + H]^+$. Exact mass: 316.0502.

6-(4-Chloro-2-methoxyphenoxy)-4-ethyl-2*H*-chromen-2-one (24). Starting from **18** (0.3 g, 1.2 mmol), compound **24** was obtained (0.16 g, 40% yield), mp 110−112 °C. ^1H NMR ($CDCl_3$, 300 MHz): δ 1.30 (t, J = 7.8 Hz, 3H), 2.72 (q, J = 7.2 Hz, 2H), 3.83 (s, 3H), 6.31 (s, 1H), 6.92 (dd, J = 2.2 and 8.4 Hz, 1H), 6.98 (d, J = 2.2 Hz, 1H), 7.00 (d, J = 8.4 Hz, 1H), 7.09 (dd, J = 2.2 and 8.4 Hz, 1H), 7.18 (d, J = 2.2 Hz, 1H), 7.25 (d, J = 8.4 Hz, 1H). MS (ESI^+) m/z: 331/333 $[M + H]^+$. Exact mass: 330.0557.

7-(4-Chloro-2-methoxyphenoxy)-2*H*-chromen-2-one (25). Starting from **19** (0.6 g, 2.66 mmol), compound **25** was obtained (0.2 g, 36% yield), mp 130−132 °C. ^1H NMR ($CDCl_3$, 300 MHz): δ 3.72 (s, 3H), 7.25 (d, J = 9.6 Hz, 1H), 6.66 (d, J = 2.2 Hz, 1H), 6.79 (dd, J = 2.2 and 8.4 Hz, 1H), 6.82 (dd, J = 2.2 and 8.4 Hz, 1H), 6.95 (d, J = 2.2 Hz, 1H), 6.98 (d, J = 8.4, 1H), 7.32 (d, J = 8.4 Hz, 1H), 7.62 (d, J = 9.6 Hz, 1H). MS (ESI^+) m/z: 303/305 $[M + H]^+$. Exact mass: 302,0346.

7-(4-Chloro-2-methoxyphenoxy)-4-methyl-2*H*-chromen-2-one (26). Starting from **20** (0.42 g, 1.7 mmol), compound **26** was obtained (0.3 g, 36% yield), mp 138−140 °C. ^1H NMR ($CDCl_3$, 300 MHz): δ 2.04 (s, 3H), 3.52 (s, 3H), 6.32 (s, 1H), 6.93 (dd, J = 2.2 and 8.4 Hz, 1H), 6.95 (d, J = 2.2 Hz, 1H), 7.02 (d, J = 8.4 Hz, 1H), 7.11 (dd, J = 2.2 and 8.4 Hz, 1H), 7.27 (d, J = 2.2 Hz, 1H), 7.29 (d, J = 8.4 Hz, 1H). MS (ESI^+) m/z: 317/319 $[M + H]^+$. Exact mass: 316.0502.

7-(4-Chloro-2-methoxyphenoxy)-4-ethyl-2*H*-chromen-2-one (27). Starting from **21** (0.5 g, 1.98 mmol), compound **27** was obtained (0.35 g, 52% yield), mp 140−142 °C. ^1H NMR ($CDCl_3$, 300 MHz): δ 1.33 (t, J = 7.4 Hz, 3H), 2.80 (q, J = 7.4 Hz, 2H), 3.80 (s, 3H), 6.20 (s, 1H), 6.75 (d, J = 2.2 Hz, 1H), 6.83 (d, J = 8.4 Hz, 1H), 6.90 (dd, J = 2.2 and 8.4 Hz, 1H), 7.01 (dd, J = 2.2 and 8.4 Hz, 1H), 7.09 (d, J = 2.2 Hz, 1H), 7.15 (d, J = 8.4 Hz, 1H). MS (ESI^+) m/z: 331/333 $[M + H]^+$. Exact mass: 330.0659.

3-(4-(4-Chloro-2-methoxyphenoxy)phenyl)-7-methoxy-2*H*-chromen-2-one (35). Starting from 34 (0.33 g, 1 mmol), compound **35** was obtained (0.50 g, 60% yield), mp 176−179 °C. ^1H NMR ($CDCl_3$, 300 MHz): δ 3.90 (s, 3H), 3.92 (s, 3H), 6.83 (d, J = 2.0 Hz, 1H), 6.92 (dd, J = 2.0 and 8.4 Hz, 1H), 7.04 (d, J = 2.2 Hz, 1H), 7.11 (dd, J = 8.4 and 2.2 Hz, 1H), 7.19 (d, J = 8.4 Hz, 1H), 7.25 (d, J = 8.4 Hz, 2H), 7.36−7.44 (m, 3H), 7.77 (s, 1H). MS (ESI^+) m/z: 409/411 $[M + H]^+$. Exact mass: 408.0765.

General Procedure for Methyl Ether Cleavage (3−15). A 1.0 M solution of BBr_3 in dichloromethane was slowly added to a solution of the methoxylated derivative in dry dichloromethane maintained at −70 °C under nitrogen atmosphere. The reaction mixture was stirred at the same temperature for 1 h and then at room temperature for 4 h. The mixture was cooled at 0 °C, and the reaction was quenched by adding methanol. The solvent was removed under reduced pressure, and the crude product was purified by flash column chromatography using a mixture of petroleum ether/ethyl acetate (70:30) as eluent.

6-(4-Chloro-2-hydroxyphenoxy)-2*H*-chromen-2-one (3). Starting from **22** (0.2 g, 0.66 mmol) and BBr_3 (1.0 M, 0.86 mL), compound **3** was obtained (0.18 g, 94% yield), mp 185−187 °C. ^1H NMR (CD_3COCD_3, 400 MHz): δ 6.42 (d, J = 9.6 Hz, 1H), 6.85 (dd, J = 1.8 and 8.4 Hz, 1H), 6.88 (d, J = 1.8 Hz, 1H), 7.02 (d, J = 8.4 Hz, 1H), 7.04 (d, J = 1.8 Hz, 1H), 7.20 (dd, J = 1.8 and 8.4 Hz, 1H), 7.26 (d, J = 8.4 Hz, 1H), 7.94 (d, J = 9.6 Hz, 1H). ^{13}C NMR (CD_3COCD_3, 400 MHz): δ 116.27, 118.95, 119.45, 119.53, 121.59, 122.96, 124.49, 131.67, 144.25, 145.27, 151.52, 152.64, 156.22, 161.78, 205.58. MS (ESI^+) m/z: 289/291 $[M + H]^+$. Exact mass: 288.0189.

6-(4-Chloro-2-hydroxyphenoxy)-4-methyl-2*H*-chromen-2-one (4). Starting from **23** (0.3 g, 0.95 mmol) and BBr_3 (1.0 M, 1.2 mL), compound **4** was obtained (0.28 g, 96% yield), mp 242−244 °C. ^1H NMR (CD_3COCD_3, 400 MHz): δ 2.34 (s, 3H), 6.05 (s, 1H), 6.87 (dd, J = 2.2 and 8.4 Hz, 1H), 7.02−7.05 (m, 2H), 7.32 (d, J = 2.2 Hz, 1H), 7.35 (dd, J = 2.2 and 8.4 Hz, 1H), 7.50 (d, J = 8.4 Hz, 1H), 8.90 (br, 1H). ^{13}C NMR (CD_3COCD_3, 400 MHz): δ 24.6, 109.5, 115.4, 115.8, 116.9, 120.1, 121.0, 121.2, 127.5, 128.3, 141.4, 143.9, 147.5, 152.8, 155.0, 162.0. MS (ESI^+) m/z: 303/305 $[M + H]^+$. Exact mass: 302.0346.

6-(4-Chloro-2-hydroxyphenoxy)-4-ethyl-2*H*-chromen-2-one (5). Starting from **24** (0.15 g, 0.50 mmol) and BBr_3 (1.0 M, 0.65 mL), compound **5** was obtained (0.14 g, 96% yield), mp 202−204 °C. ^1H NMR (CD_3COCD_3, 400 MHz): δ1.33 (t, J = 7.6 Hz, 3H), 2.90 (q, J = 7.6 Hz, 2H), 6.17 (s, 1H), 6.90 (dd, J = 2.0 and 8.4 Hz, 1H), 7.04 (d, J = 2.0 Hz, 1H), 7.06 (d, J = 8.4 Hz, 1H), 7.20 (dd, J = 2.0 and 8.4 Hz, 1H), 7.31 (d, J = 2.0 Hz, 1H), 7.35 (d, J = 8.4 Hz, 1H), 8.83 (br, 1H). ^{13}C

dx.doi.org/10.1021/jm400637m | J. Med. Chem. XXXX, XXX, XXX−XXX

NMR (CD_3COCD_3, 400 MHz): δ 11.1, 32.3, 109.7, 115.3, 115.9, 116.7, 120.3, 121.2, 121.5, 127.7, 128,5, 141.5, 144.0, 147.5, 152.7, 155.1, 162.5. MS (ESI^+) m/z: 317/319 $[M + H]^+$. Exact mass: 316.0502.

7-(4-Chloro-2-hydroxyphenoxy)-2*H*-chromen-2-one (6). Starting from **25** (0.20 g, 0.66 mmol) and BBr_3 (1.0 M, 0.85 mL), compound **6** was obtained (0.16 g, 84% yield), mp 207−209 °C. ^1H NMR (CD_3COCD_3, 400 MHz): δ 6.26 (d, J = 9.6 Hz, 1H), 6.77 (d, J = 2.2 Hz, 1H), 6.88 (dd, J = 2.2 and 8.4 Hz, 1H), 6.96 (dd, J = 2.2 and 8.4 Hz, 1H), 7.11 (d, J = 2.2 Hz, 1H), 7.15 (d, J = 8.4 Hz, 1H), 7.64 (d, J = 8.4 Hz, 1H), 7.94 (d, J = 9.6 Hz, 1H). ^{13}C NMR (CD_3COCD_3, 400 MHz): δ 116.29, 119.65, 119.95, 120.33, 124.19, 124.96, 125.67, 133.67, 146.28, 147.28, 151.52, 152.64, 156.22, 161.77, 205.85. MS (ESI^+) m/z: 289/291 $[M + H]^+$. Exact mass: 288.0189.

7-(4-Chloro-2-hydroxyphenoxy)-4-methyl-2*H*-chromen-2-one (7). Starting from **26** (0.30 g, 0. 95 mmol) and BBr_3 (1.0 M, 1.2 mL), compound **7** was obtained (0.27 g, 95% yield), mp 205−208 °C. ^1H NMR (CD_3COCD_3, 400 MHz): δ 2.40 (s, 3H), 6.20 (s, 1H), 6.79 (d, J = 2.2 Hz, 1H), 6.93 (dd, J = 8.4 and 2.2 Hz, 1H), 6.97 (dd, J = 8.4 and 2.2 Hz, 1H), 7.12 (d, J = 2.2 Hz, 1H), 7.14 (d, J = 8.4 Hz, 1H), 7.73 (d, J = 8.4 Hz, 1H), 8.50 (br, 1H). ^{13}C NMR (CD_3COCD_3, 400 MHz): δ 18.50, 104.27, 113.20, 115.78, 118.40, 121.10, 124.32, 127.31, 131.42, 141.74, 151.11, 153.44, 155.90, 160.53, 161.84, 205.70. MS (ESI^+) m/z: 303/305 $[M + H]^+$. Exact mass: 302.0346.

7-(4-Chloro-2-hydroxyphenoxy)-4-ethyl-2*H*-chromen-2-one (8). Starting from **27** (0.30 g, 1.0 mmol) and BBr_3 (1.0 M, 1.5 mL), compound **8** was obtained (0.28 g, 95% yield), mp 195−198 °C. ^1H NMR (CD_3COCD_3, 400 MHz): δ 1.33 (t, J = 7.6 Hz, 3H), 2.87 (q, J = 7.6 Hz, 2H), 6.17 (s, 1H), 6.79 (d, J = 1.8 Hz, 1H), 6.94 (dd, J = 1.8 and 8.4 Hz, 1H), 6.98 (dd, J = 1.8 and 8.4 Hz, 1H), 7.09 (d, J = 1.8 Hz, 1H), 7.13 (d, J = 8.4 Hz, 1H), 7.83 (d, J = 8.4 Hz, 1H), 9.32 (br, 1H). ^{13}C NMR (CD_3COCD_3, 400 MHz) δ: 10.85, 23.39, 102.61, 109.49, 111.74, 113.15, 116.63, 119.21, 122.61, 125.11, 129.65, 149.49, 154.29, 156.65, 159.11, 159.98, 202.56. MS (ESI^+) m/z: 317/319 $[M + H]^+$. Exact mass: 316.0502.

3-(4-Chloro-2-hydroxyphenoxy)-2*H*-chromen-2-one (9). Starting from **28** (0.25 g, 0.82 mmol) and BBr_3 (1.0 M, 1.1 mL), compound **9** was obtained (0.22 g, 93% yield), mp 201−204 °C. ^1H NMR (CD_3COCD_3, 400 MHz): δ 6.93 (dd, J = 2.2 and 8.4 Hz, 1H), 7.08 (d, J = 2.2 Hz, 1H), 7.17 (s, 1H), 7.19 (d, J = 8.4 Hz, 1H), 7.29−7.31 (m, 1H), 7.34 (dd, J = 1.8 and 8.0 Hz, 1H), 7.48−7.52 (m, 1H), 7.59 (dd, J = 1.2 and 8.0 Hz, 1H). ^{13}C NMR (CD_3COCD_3, 400 MHz): δ 116.29, 119.65, 120.14, 122.48, 124.65, 124.68, 127.43, 129.39, 130.47, 142.62, 144.62, 150.64, 156.18, 161.77, 205.85. MS (ESI^+) m/z: 289/291 $[M + H]^+$. Exact mass: 288.0189.

3-(4-Chloro-2-hydroxyphenoxy)-6-hydroxy-2*H*-chromen-2-one (10). Starting from **29** (0.35 g, 1.05 mmol) and BBr_3 (1.0 M, 2.7 mL), compound **10** was obtained (0.30 g, 94% yield), mp 185−188 °C. ^1H NMR (CD_3COCD_3, 400 MHz): δ 6.91 (dd, J = 2.2 and 8.4 Hz, 1H), 6.92 (d, J = 2.2 Hz, 1H), 6.96−6.99 (m, 2H), 7.03 (s, 1H), 7.05 (d, J = 2.4 1H), 7.15 (d, J = 8.4 Hz, 1H). ^{13}C NMR (CD_3COCD_3, 400 MHz): δ 116.31, 118.05, 121.11, 122.68, 125.65, 125.68, 127.42, 128.53, 130.66, 140.08, 144.62, 149.92, 155.31, 161.88, 205.92. MS (ESI^+) m/z: 305/307 $[M + H]^+$. Exact mass: 304.0139.

3-(4-Chloro-2-hydroxyphenoxy)-7-hydroxy-2*H*-chromen-2-one (11). Starting from **30** (0.15 g, 0.45 mmol) and BBr_3 (1.0 M, 1.2 mL), compound **11** was obtained (0.10 g, 73% yield), mp 195−196 °C. ^1H NMR (CD_3COCD_3, 400 MHz): δ 6.69 (d, J = 1.8 Hz, 1H), 6.72 (s, 1H), 6.77 (dd, J = 1.8 and 8.4 Hz, 1H), 6.86−6.86 (m, 1H), 6.89 (dd, J = 1.8 and 8.4 Hz, 1H), 7.95 (dd, J = 1.8 and 8.4 Hz, 1H), 7.05 (d, J = 8.4 Hz, 1H). ^{13}C NMR (CD_3COCD_3, 400 MHz): δ 116.32, 118.55, 121.42, 122.57, 125.42, 125.56, 127.12, 128.11, 131.05, 139.58, 144.52, 149.14, 155.57, 161.42, 205.54. MS (ESI^+) m/z: 305/307 $[M + H]^+$. Exact mass: 304.0139.

3-(4-Chloro-2-hydroxyphenoxy)-5,7-dihydroxy-2*H*-chromen-2-one (12). Starting from **31** (0.30 g, 0.82 mmol) and BBr_3 (1.0 M, 3.2 mL), compound **12** was obtained (0.20 g, 76% yield), mp 185−188 °C. ^1H NMR (CD_3COCD_3, 400 MHz): δ 6.98 (dd, J = 2.2 and 8.4 Hz, 1H), 7.00 (d, J = 2.2 Hz, 1H), 7.15 (d, J = 8.4 Hz, 1H), 7.25 (s, 1H), 7.35 (d, J = 1.8 Hz, 1H), 7.59 (d, J = 1.8 Hz, 1H). ^{13}C NMR (CD_3COCD_3, 400 MHz): δ 114.22, 116.98, 120.48, 121.55, 124.98, 125.68, 128.04, 128.98, 131.56, 140.25, 144.77, 149.56, 155.12, 160.21, 204.45. MS (ESI^+) m/z: 321/323 $[M + H]^+$. Exact mass: 320.0088.

3-(4-Chloro-2-hydroxyphenoxy)-4-methyl-2*H*-chromen-2-one (13). Starting from **32** (0.15 g, 0.41 mmol) and BBr_3 (1.0 M, 0.53 mL), compound **13** was obtained (0.11 g, 93% yield), mp 175−178 °C. ^1H NMR (CD_3COCD_3, 400 MHz): δ 2.59 (s, 3H), 6.93 (dd, J = 2.2 and 8.4 Hz, 1H), 7.06 (d, J = 2.2 Hz, 1H), 7.21 (d, J = 8.4 Hz, 1H), 7.24−7.29 (m, 1H), 7.31 (dd, J = 8.4 and 0.8 Hz, 1H), 7.44−7.50 (m, 1H), 7.66 (dd, J = 8.0 and 1.8 Hz, 1H). ^{13}C NMR (CD_3COCD_3, 400 MHz): δ 27.12, 111.45, 118.54, 122.68, 125.41, 125.18, 127.54, 128.29, 128.98, 131.52, 140.46, 146.05, 149.11, 154.85, 161.32, 205.32. MS (ESI^+) m/z: 303/305 $[M + H]^+$. Exact mass: 302.0346.

3-(4-Chloro-2-hydroxyphenoxy)-7-hydroxy-4-methyl-2*H*-chromen-2-one (14). Starting from **33** (0.06 g, 0.2 mmol) and BBr_3 (1.0 M, 0.26 mL), compound **14** was obtained (0.04 g, 84% yield), mp 191−193 °C. ^1H NMR (CD_3COCD_3, 400 MHz): δ 2.33 (s, 3H), 6.93 (dd, J = 2.2 and 8.4 Hz, 1H), 7.04 (d, J = 2.2 Hz, 1H), 7.24 (d, J = 8.4 Hz, 1H), 7.26−7.33 (m, 2H), 7.52 (d, J = 8.4 1H). ^{13}C NMR (CD_3COCD_3, 400 MHz): δ 27.25, 110.12, 116.57, 124.71, 125.06, 126.47, 127.99, 129.09, 129.67, 130.12, 144.24, 146.05, 149.24, 153.45, 163.35, 205.32. MS (ESI^+) m/z: 319/321 $[M + H]^+$. Exact mass: 318.0295.

3-(4-(4-Chloro-2-hydroxyphenoxy)phenyl)-7-hydroxy-2*H*-chromen-2-one (15). Starting from **35** (0.50 g, 1.2 mmol) and BBr_3 (1.0 M, 3.1 mL), compound **15** was obtained (0.4 g, 87% yield), mp 104−106 °C. ^1H NMR (CD_3COCD_3, 400 MHz): δ 6.82 (d, J = 2.0 Hz, 1H), 6.88 (dd, J = 2.0 and 8.4 Hz, 1H), 6.94 (d, J = 2.2 Hz, 1H), 6.98 (dd, J = 2.2 and 8.4 Hz, 1H), 7.12−7.17 (m,2H), 7.55 (d, J = 8.4 Hz, 2H), 7.75 (d, J = 8.4 Hz, 2H), 8.01 (s, 1H). ^{13}C NMR (CD_3COCD_3, 400 MHz): δ 103.02, 113.04, 113.84, 118.25, 118.31, 122.95,123.01, 123.68, 124.68, 125.12, 126.55, 127.11, 128.98, 130.02, 137.55, 141.75, 147.52, 151.62, 156.11, 160.42, 204.02. MS (ESI^+) m/z: 381/383 $[M + H]^+$. Exact mass: 380.0452.

Docking Models Building. The 3D coordinates of *Pf*FabI were retrieved from the Protein Data Bank (in complex with Triclosan; PDB code 1nhg). The 3D structure of coumarin ligands was built, and the geometry was optimized using the molecular modeling suite of programs Sybyl 7.3 (Tripos Inc., St. Louis, MO). Molecular docking was carried out using the default settings parameters of Gold, version 5.0.1.[33] The binding site definition included the pyridine nitrogen in the nicotinamide moiety of the NADH cofactor and every residue within 20 Å. Preliminary docking calculations on the triclosan/*Pf*FabI complex were performed using both GoldScore and ChemScore fitness functions. The ChemScore function allowed the crystallographic triclosan/*Pf*FabI binding mode to be reproduced and was therefore used to drive and rank the genetic algorithm search for the coumarin analogues of triclosan. One-hundred poses were generated for each ligand, and the docking outcomes were then submitted to cluster analysis by means of the AClAP program.[34,35]

Protein Purification and Inhibition Assay. All enzymes used in this study were expressed and purified exactly as outlined before,[36] and the corresponding inhibition assays were carried out without changes according to published procedures.[36−38]

Crystallization, Data Collection, and Structure Solution. *Pf*FabI suitable for crystallization was expressed and purified as published elsewhere.[19] Crystals of ternary complexes with enzyme, NADH, and compounds **7** and **11** were prepared by soaking. To this end, the inhibitors were dissolved in acetonitrile and the solution was directly added to the drops containing crystals of binary complexes of *Pf*FabI and NADH, and the resulting crystals were incubated for a week. Crystals of *Pf*FabI in complex with NADH were prepared using the hanging drop vapor diffusion method as described recently.[19]

Data sets of two crystals of ternary *Pf*FabI complexes were collected at 100 K as a consecutive series of 0.5° rotation images at the protein beamline PXIII (X06DA) of the Swiss Light Source (SLS) in Villigen, Switzerland, using a MAR225 CCD detector. The data sets were processed with XDS,[39] and the corresponding data set statistics are given in Supporting Information Table S1.

Both crystals of *Pf*FabI in complex with NADH and inhibitors **7** and **11**, respectively, were isomorphous to each other and to the crystals of PfFabI in complex with NAD and triclosan (PDB code 1NHG) or with

dx.doi.org/10.1021/jm400637m | *J. Med. Chem.* XXXX, XXX, XXX−XXX

NADH and a triclosan analogue (PDB code 1NNU).[19] For initial phasing, it was therefore sufficient to properly place the protein chains A and B from PDB entry 1NNU into the unit cells of the ternary *Pf*FabI complexes of this study by rigid-body refinement using the program PHENIX.[40] The crystal structure of *Pf*FabI in complex with NADH and compound **7** showed clear electron density for the cofactor and the inhibitor at both active sites of chains A and B. Subsequent iterative rounds of model building with COOT[41] and restrained maximum-likelihood refinement with BUSTER[42] and PHENIX[40] led to the final model (*R*-factor of 0.16, free *R*-factor of 0.20) with very good stereochemistry (Table S1). The crystal structure of *Pf*FabI in complex with NADH and **11** showed clear electron density maps for the bound cofactor and inhibitor at the active site of chain B. In contrast, in chain A only incomplete electron density of apparently partially bound cofactor and inhibitor was visible. Thus, at active site A, both NADH and compound **11** were tentatively modeled and refined with occupancies of 50%. The difference electron density map of the refined model still shows some uninterpretable positive peaks in the vicinity of NADH and **11**, presumably due to crystallization buffer components bound in the absence of cofactor and inhibitor. Iterative rounds of model building with COOT[41] and restrained maximum-likelihood refinement with BUSTER[42] and PHENIX[40] provided the final model (*R*-factor of 0.15, free *R*-factor of 0.20) with very good stereochemistry (Table S1).

In Vitro Assay for *P. falciparum* K1. In vitro activity against erythrocytic stages of *P. falciparum* was determined using the [^{3}H]hypoxanthine incorporation described recently.[43] The compounds and the standard drug chloroquine were tested against the chloroquine- and pyrimethamine-resistant K1 strain. IC_{50} values were calculated from graphically plotted dose−response curves.

■ ASSOCIATED CONTENT

Supporting Information

Crystallographic data, elemental analysis results, crystal structures of *Pf*FabI in complex with compounds **7** and **11**. This material is available free of charge via the Internet at http://pubs.acs.org.

Accession Codes

The coordinates for *Pf*FabI in complex with **7** and those for *Pf*FabI in complex with **11**, along with the observed structure factors, have been deposited with the Protein Data Bank with entry codes 4IGE and 4IGF, respectively.

■ AUTHOR INFORMATION

Corresponding Authors

*F.B: phone, +39-051-2099732; fax, +39-051-2099734; e-mail, federica.belluti@unibo.it.

*R.P.: phone, +41-22-3793371; fax, +41-22-3793360; e-mail, remo.perozzo@unige.ch.

Author Contributions

$^{\infty}$F.B. and R.P. contributed equally.

The manuscript was written through contributions of all authors. All authors have given approval to the final version of the manuscript.

Notes

The authors declare no competing financial interest.

■ ACKNOWLEDGMENTS

We gratefully acknowledge the excellent support of the beamline scientists of the X06DA and X06SA beamlines at the SLS, Villigen, Switzerland. The University of Bologna, Italy, is gratefully acknowledged for financial support.

■ ABBREVIATIONS USED

LS, liver stage; BS, blood stage; FAS-II, type II fatty acid synthase; *Pf*FAS-II, *Plasmodium falciparum* type II fatty acid synthase; ACP, acyl carrier protein; FabG, β-ketoacyl-ACP-reductase; FabZ, β-hydroxacyl-ACP-dehydratase; FabI, enoyl-ACP-reductase

■ REFERENCES

(1) WHO. *World Malaria Report 2010*; World Health Organization: Geneva, 2010; http://www.who.int/malaria/world_malaria_report_2010/en/index.html.

(2) Noedl, H.; Se, Y.; Schaecher, K.; Smith, B. L.; Socheat, D.; Fukuda, M. M. Evidence of artemisinin-resistant malaria in Western Cambodia. *N. Engl. J. Med.* **2008**, *359*, 2619−2620.

(3) Ekland, E. H.; Fidock, D. A. In vitro evaluations of antimalarial drugs and their relevance to clinical outcomes. *Int. J. Parasitol.* **2008**, *38*, 743−747.

(4) Greenwood, B. M.; Fidock, D. A.; Kyle, D. E.; Kappe, S. H.; Alonso, P. L.; Collins, F. H.; Duffy, P. E. Malaria: progress, perils, and prospects for eradication. *J. Clin. Invest.* **2008**, *118*, 1266−1276.

(5) Amino, R.; Giovannini, D.; Thiberge, S.; Gueirard, P.; Boisson, B.; Dubremetz, J. F.; Prevost, M. C.; Ishino, T.; Yuda, M.; Menard, R. Host cell traversal is important for progression of the malaria parasite through the dermis to the liver. *Cell Host Microbe* **2008**, *3*, 88−96.

(6) Lu, H.; Tonge, P. J. Inhibitors of FabI, an enzyme drug target in the bacterial fatty acid biosynthesis pathway. *Acc. Chem. Res.* **2008**, *41*, 11−20.

(7) Hemmer, C. J.; Holst, F. G.; Kern, P.; Chiwakata, C. B.; Dietrich, M.; Reisinger, E. C. Stronger host response per parasitized erythrocyte in *Plasmodium vivax* or *ovale* than in *Plasmodium falciparum* malaria. *Trop. Med. Int. Health* **2006**, *11*, 817−823.

(8) Baird, J. K.; Hoffman, S. L. Primaquine therapy for malaria. *Clin. Infect. Dis.* **2004**, *39*, 1336−1345.

(9) Mazier, D.; Renia, L.; Snounou, G. A pre-emptive strike against malaria's stealthy hepatic forms. *Nat. Rev. Drug Discovery* **2009**, *8*, 854−864.

(10) Tarun, A. S.; Vaughan, A. M.; Kappe, S. H. Redefining the role of de novo fatty acid synthesis in *Plasmodium* parasites. *Trends Parasitol.* **2009**, *25*, 545−550.

(11) Vaughan, A. M.; O'Neill, M. T.; Tarun, A. S.; Camargo, N.; Phuong, T. M.; Aly, A. S.; Cowman, A. F.; Kappe, S. H. Type II fatty acid synthesis is essential only for malaria parasite late liver stage development. *Cell. Microbiol.* **2009**, *11*, 506−520.

(12) Yu, M.; Kumar, T. R.; Nkrumah, L. J.; Coppi, A.; Retzlaff, S.; Li, C. D.; Kelly, B. J.; Moura, P. A.; Lakshmanan, V.; Freundlich, J. S.; Valderramos, J. C.; Vilcheze, C.; Siedner, M.; Tsai, J. H.; Falkard, B.; Sidhu, A. B.; Purcell, L. A.; Gratraud, P.; Kremer, L.; Waters, A. P.; Schiehser, G.; Jacobus, D. P.; Janse, C. J.; Ager, A.; Jacobs, W. R., Jr.; Sacchettini, J. C.; Heussler, V.; Sinnis, P.; Fidock, D. A. The fatty acid biosynthesis enzyme FabI plays a key role in the development of liver-stage malarial parasites. *Cell Host Microbe* **2008**, *4*, 567−578.

(13) Ralph, S. A.; van Dooren, G. G.; Waller, R. F.; Crawford, M. J.; Fraunholz, M. J.; Foth, B. J.; Tonkin, C. J.; Roos, D. S.; McFadden, G. I. Tropical infectious diseases: metabolic maps and functions of the *Plasmodium falciparum* apicoplast. *Nat. Rev. Microbiol.* **2004**, *2*, 203−216.

(14) Fichera, M. E.; Roos, D. S. A plastid organelle as a drug target in apicomplexan parasites. *Nature* **1997**, *390*, 407−409.

(15) Colizzi, F.; Recanatini, M.; Cavalli, A. Mechanical features of *Plasmodium falciparum* acyl carrier protein in the delivery of substrates. *J.Chem. Inf. Model.* **2008**, *48*, 2289−2293.

(16) Zhang, Y. M.; Lu, Y. J.; Rock, C. O. The reductase steps of the type II fatty acid synthase as antimicrobial targets. *Lipids* **2004**, *39*, 1055−1060.

(17) Surolia, A.; Ramya, T. N.; Ramya, V.; Surolia, N. "FAS"t inhibition of malaria. *Biochem. J.* **2004**, *383*, 401−412.

(18) Waller, R. F.; Ralph, S. A.; Reed, M. B.; Su, V.; Douglas, J. D.; Minnikin, D. E.; Cowman, A. F.; Besra, G. S.; McFadden, G. I. A type II pathway for fatty acid biosynthesis presents drug targets in *Plasmodium falciparum*. *Antimicrob. Agents Chemother.* **2003**, *47*, 297−301.

(19) Perozzo, R.; Kuo, M.; Sidhu, A. S.; Valiyaveettil, J. T.; Bittman, R.; Jacobs, W. R., Jr.; Fidock, D. A.; Sacchettini, J. C. Structural elucidation

of the specificity of the antibacterial agent triclosan for malarial enoyl acyl carrier protein reductase. *J. Biol. Chem.* **2002**, *277*, 13106−13114.
(20) Bhargava, H. N.; Leonard, P. A. Triclosan: applications and safety. *Am. J. Infect. Control* **1996**, *24*, 209−218.
(21) Heath, R. J. Bacterial fatty-acid biosynthesis: an antibacterial drug target waiting to be exploited. *Drug Discovery Today* **2001**, *6*, 715.
(22) McMurry, L. M.; McDermott, P. F.; Levy, S. B. Genetic evidence that InhA of *Mycobacterium smegmatis* is a target for triclosan. *Antimicrob. Agents Chemother.* **1999**, *43*, 711−713.
(23) Heath, R. J.; Li, J.; Roland, G. E.; Rock, C. O. Inhibition of the *Staphylococcus aureus* NADPH-dependent enoyl-acyl carrier protein reductase by triclosan and hexachlorophene. *J. Biol. Chem.* **2000**, *275*, 4654−4659.
(24) Surolia, N.; Surolia, A. Triclosan offers protection against blood stages of malaria by inhibiting enoyl-ACP reductase of *Plasmodium falciparum*. *Nat. Med.* **2001**, *7*, 167−173.
(25) McLeod, R.; Muench, S. P.; Rafferty, J. B.; Kyle, D. E.; Mui, E. J.; Kirisits, M. J.; Mack, D. G.; Roberts, C. W.; Samuel, B. U.; Lyons, R. E.; Dorris, M.; Milhous, W. K.; Rice, D. W. Triclosan inhibits the growth of *Plasmodium falciparum* and *Toxoplasma gondii* by inhibition of apicomplexan Fab I. *Int. J. Parasitol.* **2001**, *31*, 109−113.
(26) Chhibber, M.; Kumar, G.; Parasuraman, P.; Ramya, T. N.; Surolia, N.; Surolia, A. Novel diphenyl ethers: design, docking studies, synthesis and inhibition of enoyl ACP reductase of *Plasmodium falciparum* and *Escherichia coli*. *Bioorg. Med. Chem.* **2006**, *14*, 8086−8098.
(27) Freundlich, J. S.; Anderson, J. W.; Sarantakis, D.; Shieh, H. M.; Yu, M.; Valderramos, J. C.; Lucumi, E.; Kuo, M.; Jacobs, W. R., Jr.; Fidock, D. A.; Schiehser, G. A.; Jacobus, D. P.; Sacchettini, J. C. Synthesis, biological activity, and X-ray crystal structural analysis of diaryl ether inhibitors of malarial enoyl acyl carrier protein reductase. Part 1: 4′-Substituted triclosan derivatives. *Bioorg. Med. Chem. Lett.* **2005**, *15*, 5247−5252.
(28) Freundlich, J. S.; Yu, M.; Lucumi, E.; Kuo, M.; Tsai, H. C.; Valderramos, J. C.; Karagyozov, L.; Jacobs, W. R., Jr.; Schiehser, G. A.; Fidock, D. A.; Jacobus, D. P.; Sacchettini, J. C. Synthesis and biological activity of diaryl ether inhibitors of malarial enoyl acyl carrier protein reductase. Part 2: 2′-Substituted triclosan derivatives. *Bioorg. Med. Chem. Lett.* **2006**, *16*, 2163−2169.
(29) Borges, F.; Roleira, F.; Milhazes, N.; Santana, L.; Uriarte, E. Simple coumarins and analogues in medicinal chemistry: occurrence, synthesis and biological activity. *Curr. Med. Chem.* **2005**, *12*, 887−916.
(30) DeSimone, R. W.; Currie, K. S.; Mitchell, S. A.; Darrow, J. W.; Pippin, D. A. Privileged structures: applications in drug discovery. *Comb. Chem. High Throughput Screening* **2004**, *7*, 473−494.
(31) Meyer, T. E.; Cusanovich, M. A. Discovery and characterization of electron transfer proteins in the photosynthetic bacteria. *Photosynth. Res.* **2003**, *76*, 111−126.
(32) Cristau, H.-J.; Cellier, P. P.; Hamada, S.; Spindler, J.-F.; Taillefer, M. A general and mild Ullmann-type synthesis of diaryl ethers. *Org. Lett.* **2004**, *6*, 913−916.
(33) Jones, G.; Willett, P.; Glen, R. C. Molecular recognition of receptor sites using a genetic algorithm with a description of desolvation. *J. Mol. Biol.* **1995**, *245*, 43−53.
(34) Bottegoni, G.; Cavalli, A.; Recanatini, M. A comparative study on the application of hierarchical-agglomerative clustering approaches to organize outputs of reiterated docking runs. *J. Chem. Inf. Model.* **2006**, *46*, 852−862.
(35) Bottegoni, G.; Rocchia, W.; Recanatini, M.; Cavalli, A. AClAP, autonomous hierarchical agglomerative cluster analysis based protocol to partition conformational datasets. *Bioinformatics* **2006**, *22*, e58−e65.
(36) Tasdemir, D.; Lack, G.; Brun, R.; Ruedi, P.; Scapozza, L.; Perozzo, R. Inhibition of *Plasmodium falciparum* fatty acid biosynthesis: evaluation of FabG, FabZ, and FabI as drug targets for flavonoids. *J. Med. Chem.* **2006**, *49*, 3345−3353.
(37) Kirmizibekmez, H.; Calis, I.; Perozzo, R.; Brun, R.; Donmez, A. A.; Linden, A.; Ruedi, P.; Tasdemir, D. Inhibiting activities of the secondary metabolites of *Phlomis brunneogaleata* against parasitic protozoa and plasmodial enoyl-ACP reductase, a crucial enzyme in fatty acid biosynthesis. *Planta Med.* **2004**, *70*, 711−717.
(38) Tasdemir, D.; Brun, R.; Perozzo, R.; Dönmez, A. A. Evaluation of antiprotozoal and plasmodial enoyl-ACP reductase inhibition potential of turkish medicinal plants. *Phytother. Res.* **2005**, *19*, 162−166.
(39) Kabsch, W. Automatic processing of rotation diffraction data from crystals of initially unknown symmetry and cell constants. *J. Appl. Crystallogr.* **1993**, *26*, 795−800.
(40) Adams, P. D.; Afonine, P. V.; Bunkoczi, G.; Chen, V. B.; Davis, I. W.; Echols, N.; Headd, J. J.; Hung, L. W.; Kapral, G. J.; Grosse-Kunstleve, R. W.; McCoy, A. J.; Moriarty, N. W.; Oeffner, R.; Read, R. J.; Richardson, D. C.; Richardson, J. S.; Terwilliger, T. C.; Zwart, P. H. PHENIX: a comprehensive Python-based system for macromolecular structure solution. *Acta Crystallogr., Sect. D: Biol. Crystallogr.* **2010**, *66*, 213−221.
(41) Emsley, P.; Lohkamp, B.; Scott, W. G.; Cowtan, K. Features and development of Coot. *Acta Crystallogr., Sect. D: Biol. Crystallogr.* **2010**, *66*, 486−501.
(42) Bricogne, G.; Blanc, E.; Brandl, M.; Flensburg, C.; Keller, P.; Paciorek, W.; Roversi, P.; Sharff, A.; Smart, O. S.; Vonrhein, C.; Womack, T. O. *BUSTER*, version 2.11.2; Global Phasing Ltd.: Cambridge, U.K., 2011.
(43) Tasdemir, D.; Sanabria, D.; Lauinger, I. L.; Tarun, A.; Herman, R.; Perozzo, R.; Zloh, M.; Kappe, S. H.; Brun, R.; Carballeira, N. M. 2-Hexadecynoic acid inhibits plasmodial FAS-II enzymes and arrests erythrocytic and liver stage *Plasmodium* infections. *Bioorg. Med. Chem.* **2010**, *18*, 7475−7485.